J. Synchrotron Rad. (1998). **5**, 1082–1084

The white-radiation dynamic topography experimental system at the BSRF

G. L. Wang,* J. H. Jiang, Y. L. Tian, Y. Han and Z. G. Wang

BSRF, Institute of High Energy Physics, The Chinese Academy of Sciences, People's Republic of China. E-mail: wanggl@bepc3.ihep.ac.cn

(*Received 4 August 1997; accepted 18 November 1997*)

A white-radiation dynamic topography experimental system has been established at the BSRF (Beijing Synchrotron Radiation Facility) and is now in operation. Each part of this system is described in this paper, with particular emphasis given to the PC-based online control system, the X-ray video-imaging system and the image-treatment system. Moreover, some of the experimental results, such as the phase transition of $KNbO_3$ nonlinear optical crystals and of blue bronze charge-density-wave material, are briefly presented.

Keywords: topography; dynamic experiment; control; image treatment.

1. Introduction

The X-ray topography station and associated 4W1A beamline are part of the Beijing Synchrotron Radiation Facility (BSRF), which employs synchrotron radiation from the Beijing Electron Positron Collider (BEPC) for the study of the perfection of single crystals, high-resolution multi-crystal diffraction and X-ray standing waves. A synchrotron radiation source has many advantages for topography experiments compared with a conventional X-ray source. The high intensity of synchrotron radiation reduces exposure times from hours to seconds, making it easier to study dynamic and survey experiments. The small angular divergence of synchrotron radiation allows the specimen to be set further from the source to gain better resolution, and also allows the specimen–film distance to be increased, maintaining an acceptable resolution. Therefore, various kinds of sample chamber can be used to study the effects of a change in temperature, stress, electric field or magnetic field on crystals. Moreover, a real-time image-processing system allows direct observation of dynamic experiments.

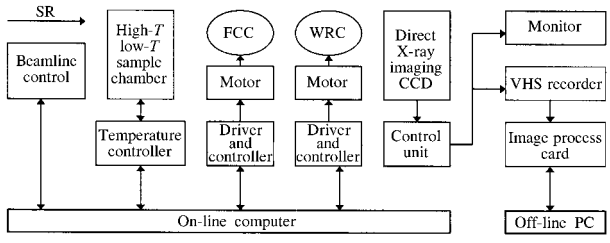

Figure 1
A schematic diagram of the BSRF topography experimental system. FCC, four-crystal camera; WRC, white-radiation camera; SR, synchrotron radiation.

Table 1
The main technical parameters of the 4W1A beamline.

Beamline type	White
Acceptance angle	1 mrad (H) × 0.3 mrad (V)
Beam size at sample	45 (H) × 13 (V) mm
Flux	6×10^{10} photons s^{-1} mA^{-1} $mrad^{-2}$ (0.1% bandwidth)$^{-1}$
Spectral range	0.3–3.7 Å

In this paper, we describe the white-radiation dynamic topography experimental system and some results of its recent research application at the BSRF. A schematic view of the experimental system is presented in Fig. 1; it consists of a white-radiation topography camera, high- and low-temperature-environment chambers, an X-ray video-imaging system and an image-capture/treatment system. These are installed inside an interlocked hutch 3 m wide and 6 m long.

2. Beamline

The experimental station (Jiang *et al.*, 1993) is located at the end of the wiggler beamline 4W1A; the distance from the specimen stage to the source is 45 m. The main parameters of the beamline are listed in Table 1. When the BEPC is operated at an energy of 2.2 GeV and the magnetic field of the wiggler is 1.8 T, the photon flux at 1.54 Å is 6×10^{10} photons s^{-1} mA^{-1} $mrad^{-2}$ (0.1% bandwidth)$^{-1}$ and the electron beam size at the source point is 2.2 × 0.8 mm. For a distance of 50 mm from specimen to film, the spatial resolution is about 3 μm (H) × 1 μm (V).

The beamline is equipped with two water-cooled slits used for defining the incident-beam size and an ion chamber for monitoring the incident-beam intensity. The slits are driven by four-phase stepping motors and controlled by an SMC-2 interface (Wang *et al.*, 1996). The signals of the X-ray intensity pass through the amplifier and discriminator and become the standard TTL (transistor–transistor logic) pulses, which then feed into the SMC-2 interface. The SMC-2 interface is a standard PC ISA (industry standard architecture) bus interface, developed by ourselves, and used for stepping-motor control and as a timer/scalar, which has one timer channel, three scalar channels and can control eight motors simultaneously.

3. Experimental system

3.1. *White-radiation topography camera*

The white-radiation camera (Bowen *et al.*, 1982), made in the UK, has five rotary axes. The specimen is rotatable on three axes to any orientation with respect to the incident beam, and the detector is rotatable up to 140° (2θ) on two axes to collect the diffracted beam. The axes and their motors are designed to allow very rapid rotation speeds, up to 90° s^{-1}, for special experiments.

3.2. *Online control and data acquisition*

The online control and data-acquisition system is based on a P/100 personal computer and plug-in cards. The tasks include controlling the beamline, the topography camera and the temperature of the sample chamber. These tasks are run on a Windows95 platform.

The white-radiation camera and the four-crystal camera have many rotating axes. These axes are used to coincide with the incident beam and to adjust the specimen and detector to any position. All axes are driven by stepping motors and run in open-

loop control. An IEEE-488 stepping-motor controller and a plug-in IEEE-488 interface are used for motor control.

The station is equipped with two high-temperature-environment chambers and one low-temperature chamber for different experiments. One of the high-temperature chambers ('heavy') is multi-functional, but is difficult to align, and is used at temperatures greater than 1273 K. The second one ('light') is simple and easy to handle, and is used in the medium temperature range. The temperature-control system is based on the Eurotherm controller (Eurotherm Ltd, 1995) and solid-state relay. By using PID (proportional, integral and differential) control and the time-proportion method, the temperature resolution is about 0.05 K at hold range and 0.01 K at ramp, dwell range. The online computer can set and monitor the temperature through the RS-232 interface.

3.3. *Detector and image treatment*

Besides the X-ray film, a Siemens CCD (charge-coupled device) (type XQ1177) is used to convert the X-rays directly to electrical signals with a spatial resolution of 25 μm. The CCD amplify/control unit outputs three channels of standard video signals, one to a high-resolution monitor for real-time display, one to a VHS recorder for recording and another to the computer for online image treatment.

The image-capture/treatment system is based on a P/100 personal computer and a newly developed PCI (peripheral connect interface) bus plug-in card, which is used for modest resolution, real-time display and processing during dynamic experiments. The treatment of images can be performed either online or post-acquisition. Some simple functions, such as contrast reverse and noise reduction by the rolling integration method, can be performed by online treatment, while a wide range of filters can be used in post-acquisition treatment to improve the quality of images recorded on VHS videotape or X-ray film.

A diagram of the image-capture/treatment card is shown in Fig. 2. The images can be captured as standard .BMP or .TIF files up to the rate of 25 frames s^{-1} with a maximum digital image resolution of 768 × 576 × 8 bits. The software was specially written for use on a Windows platform by ourselves and offers simplicity and ease of operation; moreover, the software supports Windows DDE (dynamic data exchange) and OLE (object linking and embedding), enabling data to be transferred into popular commercial software such as Photoshop or Photofinish for further processing. A substantial improvement in the image quality can be achieved after the image-processing system has been used.

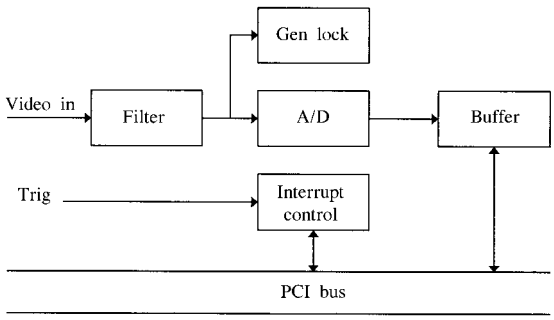

Figure 2
A sketch of the image-capture/treatment card.

4. Physical results

The dynamic topography experimental system has been put into operation and many experiments have been performed in dedicated synchrotron radiation time. Recent work includes research on ferroelastic and ferroelectric domain structure in Ba_2NaNbO_5 (BSN), $KNbO_3$ (KN), $KTa_{1-x}Nb_xO_3$ (KTN) and NdP_5O_{14} (NPP) crystals (Jiang, 1993), HgCdTe multi-line array (MLA) infrared detectors and molecular-beam-epitaxy-grown $In_xGa_{1-x}As/GaAs$ strained-layer superlattices (Cui *et al.*, 1993). Here we present some physical results on the phase transition of $KNbO_3$ nonlinear optical crystals (Zhao *et al.*, 1991) and $K_{0.3}MoO_3$ charge-density-wave (CDW) material.

Potassium niobate $KNbO_3$ exhibits outstanding nonlinear optical and electro-optical properties. Its phase transition chain is as follows:

trigonal (263 K) → orthorhombic (498 K) → tetragonal (708 K) → cubic.

We have studied domain configuration and evolution across the orthorhombic-to-tetragonal phase transition at a temperature near 498 K. Fig. 3 shows a series of synchrotron radiation topographs during heating. Only the (331) diffraction is shown here. At room temperature, the domains along the [010] and [110] directions are given in Fig. 3(*a*). At the phase-transition point (497 K), contrast was reduced, as can be seen in the diffuse image shown in Fig. 3(*b*). After the phase transition (307 K), the domains along [010] disappeared while the domains along [110] reappeared.

The whole process of the phase transition has been recorded by the video-imaging system, which confirms the evolution of the contrast of ferroelectric domains in the crystals during heating.

The layered-structure compound, blue bronze, $K_{0.3}MoO_3$, is a typical model material with charge-density waves; it is a quasi-

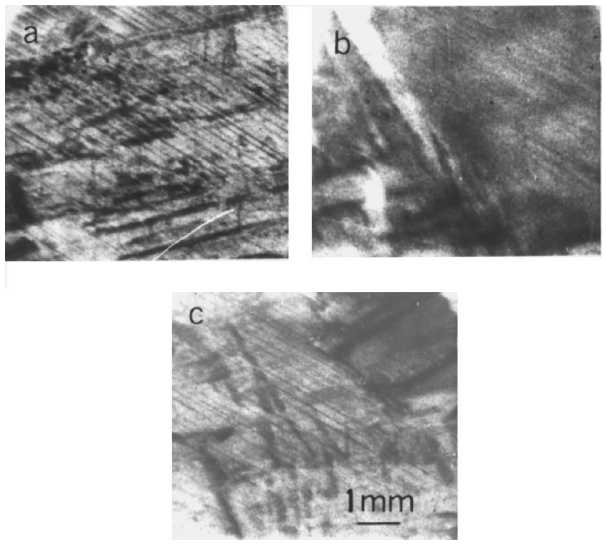

Figure 3
Synchrotron radiation topographs of the phase transitions in KN, (331) reflection. (*a*) At room temperature (297 K), (*b*) at the phase-transition point (497 K), (*c*) after the transition (307 K).

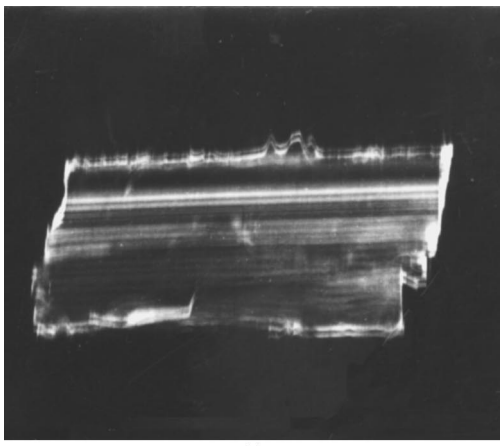

(*a*)

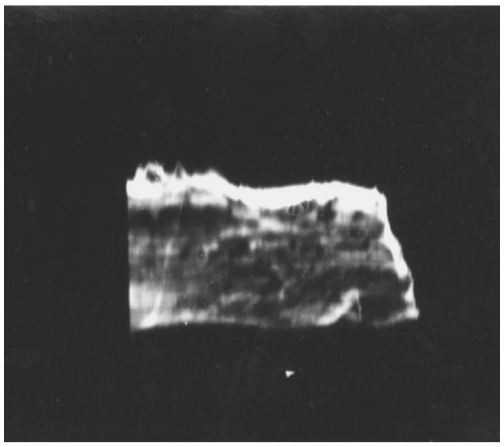

(*b*)

Figure 4
Synchrotron white-beam topographs of the phase transition in blue bronze $K_{0.3}MoO_3$, $(2\bar{3}1)$ reflection. (*a*) At room temperature, (*b*) at liquid-nitrogen temperature (77 K).

one-dimensional conductor at room temperature and undergoes a metal–semiconductor transition at 180 K, which is known to be a Peierls transition and is accompanied by the formation of CDWs connected with the $2K_F$ periodic lattice distortion. The sliding transport of a CDW is not free, but is strongly damped due to the pinning effects of defects or other impurities. When the electric field exerted on the sample is less than the critical value E_T, the CDW is still pinned and cannot carry current; thus the d.c. conductivity has a normal ohmic behaviour. At $E > E_T$, the CDW depinned by the applied field can be driven into current-carrying states, leading to nonlinear transport. By using synchrotron radiation white-beam topography, we observed the phase transition of $K_{0.3}MoO_3$ at low temperature. Fig. 4 shows the photographs obtained, (*a*) at room temperature and (*b*) at liquid-nitrogen temperature (77 K). The images observed indicate that a number of defects and domain structures exist in the sample, and accompanying the phase transition, there are some changes in defects, domain structure and crystal plane orientations. This reflects the fact that the formation and transport properties of CDWs are closely related not only to the defects and domain structures, but also to the distortion of crystal planes.

The authors would like to thank Dr Zhao Jiyong and Professor Jiang Xiaoming for their contributions to the work.

References

Bowen, D. K., Clark, G. F., Davies, S. T., Nicholson, J. R. S., Roberts, K. J., Sherwood, J. N. & Tanner, B. K. (1982). *Nucl. Instrum. Methods*, **195**, 277–284.

Cui, S. F., Wang, G. M., Mai, Z. H., Feng, W., Li, C. R., Dai, D. Y., Li, J. H. & Zhou, J. M. (1993). *Phys. Rev. B*, **48**, 8797–8800.

Eurotherm Ltd. (1995). *818 Controller/Programmer Installation Instructions*, pp. 15–18. Durrington, Worthing, West Sussex BN13 3PL, England.

Jiang, S. S. (1993). *Ferroelectrics*, **140**, 71–78.

Jiang, J. H., Zhao, J. Y., Tian, Y. L., Han, Y., Chao, Z. Y., Jiang, X. M. & Xian, D. C. (1993). *Nucl. Instrum. Methods A*, **366**, 354–360.

Wang, G. L., Jiang, J. H., Tian, Y. L. & Han, Y. (1996). *Nucl. Tech.* **20**, 239–241. (In Chinese.)

Zhao, J. Y., Yang, P., Jiang, S. S., Jiang, X. M., Jiang, J. H. & Xian, D. C. (1991). *Appl. Phys. Lett.* **59**, 1952–1954.